Small-Angle X-ray Scattering Analyses of Lamellar Microdomains Based on a Model of One-Dimensional Paracrystal with Uniaxial Orientation

Mitsuhiro Shibayama† and Takeji Hashimoto*

Department of Polymer Chemistry, Kyoto University, Kyoto 606, Japan.
Received May 15, 1985

ABSTRACT: Small-angle X-ray scattering (SAXS) from polystyrene–polyisoprene diblock polymer films in which the lamellar microdomains have a high degree of orientation was studied both experimentally and theoretically. Experimental SAXS profiles were measured with a point collimation in order to circumvent complicated slit desmearing procedures for the oriented systems and were compared with the theoretical profiles derived on the basis of a *preferentially oriented* one-dimensional paracrystal model. The observed scattered intensity $J(h,\mu)$ at a given azimuthal angle μ and magnitude of scattering vector, h, was shown to be given by $J(h,\mu) \sim h^{-2}I_1(h)$, irrespective of sharpness of the orientation distribution under the usual conditions where the lateral dimension of the lamellae is much larger than the thickness of each lamella. Here $I_1(h)$ is the scattered intensity for the perfectly oriented system along the direction perpendicular to the lamellar interfaces, whose asymptotic behavior is given by $h^{-2}\exp(-\sigma^2h^2)$, where σ is the parameter associated with the domain boundary thickness. The formula for $J(h,\mu)$ was proven to be correct both by numerical calculations and by the experimental SAXS profiles. Comparisons between the theoretical and experimental profiles give quantitative estimations of various fundamental structural parameters of the microdomains, including the domain boundary thickness.

I. Introduction

Block polymers form microdomain structures. The size of the microdomains perpendicular to the interfaces is of the order of several tens of nanometers,[1] as determined by electron microscopy and small-angle X-ray and neutron scattering.

The domain identity period and the domain size are found to be closely related to the molecular parameters of the block polymers (such as the molecular weight, the statistical segment length, and the Flory–Huggins interaction parameter χ_{AB} between constituent block chains A and B.[1e,2,3] The molecular weight dependence of the domain identity period and the domain size were studied for lamellar,[1a,2b,3-7] cylindrical,[7-9] and spherical microdomain systems.[7,10-12] The equilibrium and nonequilibrium aspects of the microdomain systems were investigated, and the experimental results in the equilibrium regime were found to be predictable in terms of equilibrium statistical mechanical theories.[13-15]

The interfacial thickness, which is also an important structural parameter of the system, has been studied by a number of workers by scattering methods.[1e] The methods involve either the best fitting of experimental scattering profiles with theoretical profiles[16] or analyses of the systematic deviation of the small-angle scattering curve at the large-angle tail from Porod's rule due to finite interfacial thickness.[5,11,12,17,18,20-30] The latter method is useful to determine *the narrow interfacial thickness* but is not appropriate for systems with a *broad interfacial region* that invokes a significant reduction of the scattered intensity in the angular region where Porod's rule is applicable. For systems with a broad interfacial region, the former method is more appropriate than the latter and becomes very powerful, especially when the scattering curves exhibit a number of scattering maxima, as is usually found in block polymer systems.[5,11,16,19] Tapered block polymers[31] and block polymers in solutions[13-15] are typical systems that have a broad interfacial region. Thus, the theoretical investigations of scattering behavior from the microdomain systems and quantitative comparisons of the theoretical curves with the experimental ones are of importance to determine the fundamental structural parameters, as will be described in this paper.

As for the scattering analyses of lamellar microdomain systems, Sadron and Gallot[1b] and Skoulios[19] pursued systematic studies on the concentration and temperature dependence of lamellar thicknesses. Skoulios presented a method to evaluate interfacial thickness from the intensity ratio of the multiple-order scattering maxima.[19] Hoffmann and his co-workers[1a] carried out systematic studies on the molecular weight dependence of the lamellar identity period. In most of these studies, the scattering method had been used to identify angular positions of the scattering maxima, but the entire scattering profiles and their changes with temperature and concentration had neither been presented nor discussed quantitatively.

We presented entire scattering profiles from the lamellar microdomain systems and found multiple-order scattering maxima,[16] which contained rich information about the structure of the microdomain systems. Experimental SAXS profiles were compared with theoretical ones derived from a one-dimensional paracrystal model, from which structural information such as the average domain identity period $\bar{D}$, its root mean square fluctuations ΔD, the volume fraction of one type of the domain ϕ (e.g., polystyrene), and "the characteristic interfacial thickness[5] t" were obtained.[16] In later work the thickness t was determined more quantitatively by analyzing systematic deviations of SAXS profiles at the large-angle tail from Porod's rule.[5,11,22-24,28] Structural parameters such as $\bar{D}$ and t were investigated as a function of molecular weight of block polymers, the results of which were quantitatively compared with those predicted from equilibrium statistical mechanical theories.[5]

Our earlier analyses of lamellar microdomain systems were based on the assumption of *perfect orientation of lamellar normals* along the film normal.[5,16,22] The assumption was made on the basis of the experimental evidence that the second-order orientation factor f_α as defined by

$$f_\alpha = [3\langle\cos^2\alpha\rangle - 1]/2 \qquad \text{(I-1)}$$

was typically 0.95, indicating almost perfect orientation of the lamellar microdomains (α being the polar angle

†Present address: Department of Polymer Science and Engineering, Kyoto Institute of Technology, Matsugasaki, Kyoto 606, Japan.

0024-9297/86/2219-0740$01.50/0

between the film normal and the lamellar normal).[5,22]

In this paper we critically test the assumption of the perfect orientation and come to the conclusion briefly described below. Our earlier analyses showed that the scattering intensity profile $I_1(h)$ along the lamellar normal from the perfectly oriented systems has an asymptotic behavior, as given by[5,22]

$$I_1(h) \sim h^{-2} \exp(-\sigma^2 h^2) \quad \text{(I-2)}$$

where h is the magnitude of the scattering vector as defined by

$$h = (4\pi/\lambda) \sin \vartheta \quad \text{(I-3)}$$

and 2ϑ and λ are the scattering angle and wavelength of radiation, respectively. For systems having preferred orientation and those in which the lateral dimensions of lamellae are much greater than their thicknesses, the observed scattering intensity $J(h,\mu)$ at a given azimuthal angle direction μ was found to be given by

$$J(h,\mu) \sim h^{-2} I_1(h) \quad \text{(I-4a)}$$

and hence to have the asymptotic behavior at large h as given by

$$J(h,\mu) \sim h^{-4} \exp(-\sigma^2 h^2) \quad \text{(at large } h\text{)} \quad \text{(I-4b)}$$

irrespective of sharpness of the orientation distribution except for the perfect orientation (see section II-4). Equation I-4b was confirmed by a numerical method and by experimental SAXS profiles (see sections II-5 and III-3) and was further used to evaluate the structural parameters (see section III-3).

It has come to our attention that Annighofer and Gronski[32] recently investigated the interfacial thickness as well as the domain identity period of lamellar microdomains of special block polymers with a random sequence between pure block chains based on simulations of the experimental SAXS profiles obtained with a slit collimation with the theoretical profiles derived from eq I-4a.

In a sense our work is on the same line as theirs. However, we shall focus our attention (i) on showing that eq I-4 is theoretically (both analytically and numerically) valid irrespective of the sharpness of the orientation distribution and (ii) on using eq I-4 for simulations of the SAXS profiles obtained with *point collimation* to determine the interfacial thickness and other structural parameters for pure diblock polymers. We believe that the use of point collimation is particularly important because our preliminary work based on simulations show that the slit-height smearing effect alters the relationship given by eq I-4.[33]

II. Theoretical Section

In this section we shall first derive a scattering formula for the lamellar microdomains with preferred orientation (section II-3). Then the Lorentz factor (e.g., h^{-2} in eq I-4a) and Porod's rule (eq I-4b) will be derived (section II-4) for uniaxially oriented lamellar microdomain systems in which *the lateral dimensions of the domains are much greater than their thicknesses*. The theoretical result will be confirmed in section II-5.

1. Model. Figure 1 shows a model; the structural unit is a disk of thickness L_j and radius R. The disks are stacked one-dimensionally with their centers along the z axis. The positional fluctuations of the centers of the disks exist only along the z axis, not perpendicular to it. The number of stacked lamellae is N, and the distance between adjacent disks is D_j. We call this stack a "grain"[41] hereafter. The shape of this grain is cylindrical of length $N\bar{D}$ and radius R, where $\bar{D}$ is the average value of D_j. The axis

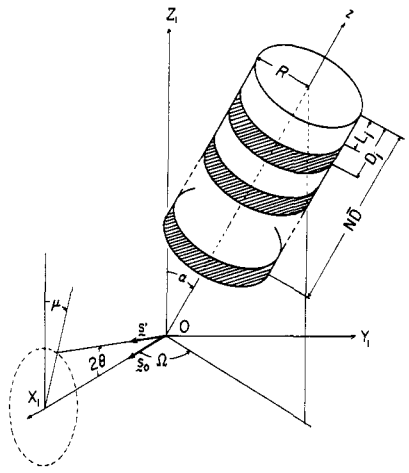

Figure 1. Model used for the simulation.

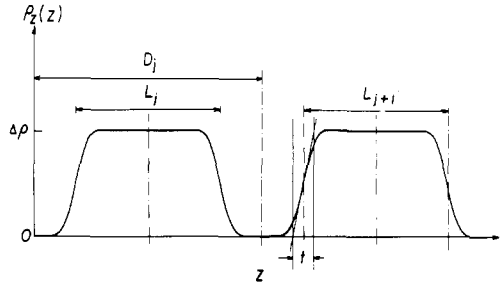

Figure 2. Model of the relative electron density variation along the z axis, $\rho_z(z)$.

of the disk z is oriented with respect to the Z_1 axis with orientation distribution function $W(\alpha,\Omega)$. The axes X_1 and Z_1 are taken in the direction parallel to the propagation direction of the incident X-ray beam as defined by the unit vector s_0 and in the direction normal to the film surfaces O–X_1Y_1, respectively. The SAXS is detected as a function of Bragg's angle 2ϑ and the azimuthal angle μ, where $\mathbf{s}'$ is a unit vector along the scattered beam.

The coordinate O–xyz is fixed to the grain. It is assumed that the electron density variation along the z axis is independent of that along the direction perpendicular to it. Therefore the electron density $\rho_j(\mathbf{r})$ within the grain is given by

$$\rho_j(\mathbf{r}) = \rho_r(x,y)\rho_{zj}(z) \quad \text{(II-1)}$$

The variation of electron density perpendicular to z axis is given by

$$\rho_r(x,y) = 1 \quad \text{for } (x^2 + y^2)^{1/2} \le R \quad \text{(II-2a)}$$

$$\rho_r(x,y) = 0 \quad \text{otherwise} \quad \text{(II-2b)}$$

On the other hand, the variation along the z axis is sigmoidal, as shown in Figure 2, and is given by

$$\rho_{zj}(z) = \rho_{zj}^{\circ}(z) * T(z) \quad \text{(II-3)}$$

$$\rho_{zj}^{\circ}(z) = \Delta\rho \quad |z| \le L_j/2$$

$$\rho_{zj}^{\circ}(z) = 0 \quad D_j/2 \ge |z| > L_j/2 \quad \text{(II-4a)}$$

$$T(z) = (2\pi\sigma^2)^{-1/2} \exp(-z^2/2\sigma^2) \quad \text{(II-4b)}$$

where asterisk denotes convolution product and $\Delta\rho$ is the excess electron density of one type of electron relative to the other.

$$u(x) * v(x) = \int u(x - x')v(x')\, dx' \quad \text{(II-5)}$$

$T(z)$ is a "smoothing function" associated with the diffuse

boundary, and σ is a parameter related to the "characteristic interfacial thickness" t

$$\sigma = (2\pi)^{-1/2}t \tag{II-6}$$

Mathematically t is nothing other than the integral breadth of the smoothing function $T(z)$. Under the condition of $R \gg L$, only the diffuse boundaries along the z axis make a significant contribution to the scattering behavior, and the boundaries in other directions make a negligible contribution because the interfacial area associated with the boundaries in other directions is negligibly small compared with that along the z axis.

2. Validity of Assumptions. Let us consider here the validity of the various assumptions employed in the model. The alternating lamellar microdomains of A and B in A–B and A–B–A block polymers are regularly organized in space:[1a-e] the domain thicknesses D_A and D_B and the domain identity period $D = D_A + D_B$ are quite uniform, the ratio of the weight-average and number-average domain identity periods $\bar{D}_w/\bar{D}_n$ being shown to be 1.001,[39] and thus the interfaces between A and B lamellae are highly parallel. Moreover the interfaces are quite flat and not wavy. Even if waviness exists, the root mean square displacement of the interfaces along the z direction in Figure 1 (i.e., along the lamellar normal), which results from the waviness, is much smaller than the average lamellar thicknesses D_A and D_B from the electron microscopic observations (see, for example, Figure 3 of ref 39). Consequently the assumption that the electron density variation along the z axis is independent of that along the direction perpendicular to it is legitimate to our systems. The extent of the lamellae parallel to the interfaces extends at least over a few tens of microns[39] and is much larger than D_A, D_B, and D, which are of order of a few tens of nanometers, the condition of $R \gg L$ being therefore satisfied.

3. Scattering Formula from Lamellar Microdomains with Preferred Orientation. Let us consider the scattering amplitude $a(h;\alpha,\Omega)$ from a disk whose axis z has an orientation (α,Ω) with respect to $O\text{–}X_1Y_1Z_1$ coordinate

$$a(\mathbf{h};\alpha,\Omega) = A_e\int \rho(\mathbf{r}) \exp(-i\mathbf{h}\cdot\mathbf{r})\, d\mathbf{r} \tag{II-7}$$

where A_e is the scattering amplitude from an electron. Noting that

$$\mathbf{h} = 2\pi\mathbf{s} = 2\pi(\mathbf{s}_0 - \mathbf{s}')/\lambda = h_x\mathbf{i} + h_y\mathbf{j} + h_z\mathbf{k} \tag{II-8}$$

and that

$$\mathbf{r} = x\mathbf{i} + y\mathbf{j} + z\mathbf{k} \tag{II-9}$$

and carrying out the integration of eq II-7, one obtains

$$a(\mathbf{h};\alpha,\Omega) = 2VA_e\Delta\rho\left(\frac{J_1(w)}{w}\right)\left(\frac{\sin(h_zL/2)}{h_zL/2}\right)\exp(-\sigma^2h_z^2/2) \tag{II-10a}$$

where

$$w = (h_x^2 + h_y^2)^{1/2} \tag{II-10b}$$

J_1 is the Bessel function of the first kind of order 1, V is the volume of the disk, and $\Delta\rho$ is the excess electron density of the disk with respect to the medium.

Taking into account the interference between the disks, *the scattered intensity from the single grain oriented at* (α,Ω) is given by

$$I(\mathbf{h};\alpha,\Omega) = \sum_{j,k=1}^{N}\langle a_ja_k^* \exp(-ih_zz_{jk})\rangle \tag{II-11a}$$

$$I(\mathbf{h};\alpha,\Omega) = C\sum_{j,k}^{N}\langle f_jf_k^* \exp(-ih_zz_{jk})\rangle \tag{II-11b}$$

where z_{jk} is the distance between the jth and kth disks and a^* and f^* stand for the complex conjugates of a and f, respectively. The quantities C and f_j are respectively given by

$$C = 4V^2A_e^2\Delta\rho^2[J_1(w)/w]^2 \tag{II-12}$$

$$f_j = \frac{\sin(h_zL_j/2)}{h_zL_j/2}\exp(-\sigma^2h_z^2/2) \tag{II-13}$$

and the symbol $\langle\ \rangle$ denotes ensemble average. Following a standard calculational procedure developed by Hosemann and Bagchi[34] for the one-dimensional paracrystal as characterized by Gaussian distance statistics $H_1(z)$

$$H_1(z) = (2\pi\Delta D^2)^{-1/2}\exp[-(z - \bar{D})^2/2(\Delta D)^2] \tag{II-14}$$

where $\bar{D}$ and ΔD are the average and the standard deviation of the interlamellar distance D, respectively, one obtains

$$I(\mathbf{h};\alpha,\Omega) = 4NV^2\Delta\rho^2A_e^2[J_1(w)/w]^2\mathcal{J}_1(h_z;\alpha,\Omega) \tag{II-15}$$

$$\mathcal{J}_1(h_z;\alpha,\Omega) = [\langle|f|^2\rangle - |\langle f\rangle|^2] + |\langle f\rangle|^2[Z + I_c/N] \tag{II-16}$$

where Z is the lattice factor given by

$$Z = \mathrm{Re}\,[(1 + F)/(1 - F)] = \frac{1 - |F|^2}{1 - 2|F|\cos(h_z\bar{D}) + |F|^2} \tag{II-17}$$

and F is given by the Fourier transformation of the distance statistics, i.e., $H_1(z)$

$$F(h_z) = |F(h_z)|\exp(-ih_z\bar{D}) \tag{II-18}$$

with

$$|F(h_z)| = \exp[-(\Delta D)^2h_z^2/2] = \exp[-g^2\bar{D}^2h_z^2/2] \tag{II-19}$$

The quantity g is Hosemann's "g factor" defined as $g = \Delta D/\bar{D}$. The lattice factor Z has maxima at $h_z\bar{D} = 2n\pi$ ($n = 1, 2, 3, \ldots$). The term I_c is the one that contributes to the zeroth order scattering intensity and is given by

$$I_c(h_z) = \{-2|F|[1 + |F|^2]\cos(h_z\bar{D}) - 2|F| - |F|^N\cos[(N + 1)h_z\bar{D}] + 2|F|^{N+1}\cos(Nh_z\bar{D}) - |F|^{N+2}\cos[(N + 1)h_z\bar{D}]\}/[1 - 2|F|\cos(h_z\bar{D}) + |F|^2] \tag{II-20}$$

In the case where N is large, I_c is important only at $h \simeq 0$.

If the grains are uniaxially oriented with respect to the Z_1 axis, *the observed intensity profile at a particular* μ, $J(h,\mu)$, is given by summing the intensity of $I(\mathbf{h};\alpha,\Omega)$ over all grains[42]

$$J(h,\mu) = \int_0^{\pi/2}\int_0^{2\pi} I(h,\mu;\alpha,\Omega)W(\alpha,\Omega)\sin\alpha\, d\alpha\, d\Omega \tag{II-21a}$$

where $W(\alpha,\Omega)$ specifies the orientation distribution function of the grains with

$$\int_0^{\pi/2}\int_0^{2\pi} W(\alpha,\Omega)\sin\alpha\, d\alpha\, d\Omega = G \tag{II-21b}$$

G is the total number of the grains.

4. Lorentz Factor and Porod's Rule for Oriented Systems. In the case when $R \gg \lambda$, the condition being normally satisfied in the experimental systems as discussed in section II-2, $J_1(w)/w$ in eq II-15 has a nontrivial value only at the limit of

$$h_r = (h_x^2 + h_y^2)^{1/2} \rightarrow 0 \quad \text{(II-22)}$$

Hence

$$[J_1(w)/w]^2 \rightarrow {}^1/_4\delta(h_r) \quad \text{(II-23)}$$

where $\delta(x)$ is Dirac's δ function. Thus a single grain having a given orientation gives scattering only along its own axis z. In the following discussion we shall consider only the scattering under this criterion of $R \gg \lambda$.

In the case when the grain axis has an orientation distribution given by $W(\alpha,\Omega)$, *the observed scattered intensity* $J(h,\mu)$ along the azimuthal angle μ is given by

$$J(h,\mu) = I(h)W(\alpha=\mu,\Omega=90°) \quad \text{(II-24)}$$

where $I(h)$ *is the scattered intensity from a single grain along its own axis* z and W is the number of the grains whose axis z orients in the direction as specified by (h,μ). At small h, the grain that gives rise to the scattering in the direction of (h,μ) is the one whose axis z is oriented at $\alpha = \mu$ and $\Omega = 90°$, hence resulting in eq II-24.

Consider *the theoretical scattered intensity* $I_1(h,\mu=0)$ *along the* Z_1 *axis for perfectly oriented systems where all grains of total number* G *orient along the* Z_1 *axis.* The intensity $I_1(h,\mu=0)$ should be related to the observed $J(h,\mu)$

$$I_1(h,\mu=0) = \int_0^{\pi/2} J(h,\mu)2\pi h^2 \sin\mu \, d\mu \quad \text{(II-25)}$$

for *the uniaxial orientation of the grains* with the Z_1 axis, for which $W(\alpha,\Omega)$ depends only on α. From eq II-24 and -25 it follows that

$$I_1(h,\mu=0) = I(h)h^2G \quad \text{(II-26)}$$

and

$$G = \int_0^{\pi/2} W(\alpha=\mu,\Omega=90°)2\pi \sin\mu \, d\mu \quad \text{(II-27)}$$

Hence from eq II-24 and 26

$$J(h,\mu) = (W(\alpha=\mu,\Omega=90°)/G)h^{-2}I_1(h,\mu=0) \quad \text{(II-28)}$$

Now $I_1(h,\mu=0)/G$ can be calculated from $I(\mathbf{h},\alpha,\Omega)$ in eq II-15 by setting $\mu = 0$ and $\alpha = \Omega = 0$. Under this condition

$$h_x = h_y = 0, \qquad h_z = -h \quad \text{(II-29)}$$

and $w = 0$. Hence it follows that

$$I_1(h,\mu=0)/G = NV^2\Delta\rho^2A_e^2\mathcal{J}_1(h;\alpha=0) \quad \text{(II-30)}$$

where $\mathcal{J}_1(h,\alpha=0)$ *is the scattered intensity profile of the single one-dimensional system along its own axis* as discussed in our earlier work.[16]

It should be noted that eq II-28 is essentially identical with that derived by Ruland.[35] The factor h^2 in eq II-26 and h^{-2} in eq II-28 is well-known as the *Lorentz factor.* Thus the following relationship is obviously valid, *irrespective of the degree of orientation*

$$J(h,\mu) \sim h^{-2}I_1(h,\mu=0) \quad \text{(II-31a)}$$

$$J(h,\mu) \sim h^{-2}\mathcal{J}_1(h,\alpha=0) \quad \text{(II-31b)}$$

Since

$$\lim_{h\rightarrow\infty} Z = 1 \quad \text{(II-32)}$$

and

$$\lim_{h\rightarrow\infty} (I_c/N) = 0 \quad \text{(II-33)}$$

it follows from eq II-16 and II-30 that

$$\lim_{h\rightarrow\infty} I_1(h,\mu=0) \sim \lim_{h\rightarrow\infty} \langle|f(h,\mu=0;\alpha=0)|^2\rangle \quad \text{(II-34)}$$

and by using eq II-13 and -29

$$\lim_{h\rightarrow\infty} I_1(h,\mu=0) \sim h^{-2}\exp(-\sigma^2h^2) \quad \text{(II-35a)}$$

and that

$$\lim_{h\rightarrow\infty} J(h,\mu=0) \sim h^{-4}\exp(-\sigma^2h^2) \quad \text{(II-35b)}$$

Consequently it is obvious that *Porod's rule for perfectly oriented lamellar systems* having $\sigma = 0$ is given by

$$\lim_{h\rightarrow\infty} I_1(h,\mu=0) \sim h^{-2} \quad \text{(II-36)}$$

as discussed in the previous work.[22] Porod's rule for preferentially oriented systems is given, from eq II-31 and -36, by

$$\lim_{h\rightarrow\infty} J(h,\mu) \sim h^{-4} \quad \text{(II-37)}$$

irrespective of the degree of lamellar orientation.

Equation II-31 can be obtained also by a slightly different process. From eq II-15 and -21a

$$J(h,\mu) = 4NV^2\Delta\rho^2A_e^2\int_0^{\pi/2}\int_0^{2\pi}\left\{\frac{J_1(w)}{w}\right\}^2 \mathcal{J}_1(h_z;\alpha,\Omega)W(\alpha)\sin\alpha \, d\alpha \, d\Omega \quad \text{(II-38)}$$

When the scattering vector h is greater than that giving rise to the first-order scattering maximum, $\mathcal{J}_1(h_z;\alpha,\Omega)$ depends primarily on L, the particle dimension. Since $L \ll R$, the angular dependence of $[J_1(w)/w]^2$ with α and Ω is much larger than that of $\mathcal{J}_1(h_z;\alpha,\Omega)$. Thus $J(h,\mu)$ is approximately given by

$$J(h,\mu) \simeq 4NV^2\Delta\rho^2A_e^2\mathcal{J}_1(h_z,\alpha=\Omega=0)\int_0^{\pi/2}\int_0^{2\pi}[J_1(w)/w]^2W(\alpha) \times \sin\alpha \, d\alpha \, d\Omega \quad \text{(II-39)}$$

In eq II-39

$$\mathcal{J}_1(h_z,\alpha=\Omega=0) \equiv \mathcal{J}_1(h,\alpha=0) \quad \text{(II-40)}$$

and

$$\int_0^{\pi/2}\int_0^{2\pi}[J_1(w)/w]^2W(\alpha)\sin\alpha \, d\alpha \, d\Omega \sim h^{-2} \quad \text{at } hR \gg 1 \quad \text{(II-41)}$$

since eq II-41 describes the scattering intensity from *the partially oriented infinitely thin disk*, whose asymptotic behavior is given by h^{-2}, again irrespective of the degree of orientation (as shown in section II-5). Combining eq II-39–41 and -30, one obtains eq II-31.

5. Numerical Results on Scattering Profiles. In this section we shall perform numerical calculations of eq II-38. Here we are only interested in *the meridional scattering*, i.e., the scattering at $\mu = 0$. In this case, from eq II-10b

$$w = hR\sin\alpha \qquad \text{and} \qquad h_z = -h\cos\alpha \quad \text{(II-42)}$$

Consequently eq II-38 is simplified as

$$J(h,\mu=0) = 4NV^2\Delta\rho^2A_e^2\int_0^{\pi/2}W(\alpha) \times \left\{\frac{J_1(hR\sin\alpha)}{hR\sin\alpha}\right\}^2\mathcal{J}_1(-h\cos\alpha)\sin\alpha \, d\alpha \quad \text{(II-43)}$$

$W(\alpha)$ is assumed to be given by a Gaussian function

$$W(\alpha) = c'\exp(-\alpha^2/2\sigma_\alpha^2) \quad \text{(II-44)}$$

where c' is a normalization constant satisfying eq II-27. Here the numerical calculations were performed for $\sigma_\alpha = 1°$, the corresponding second-order orientation factor de-

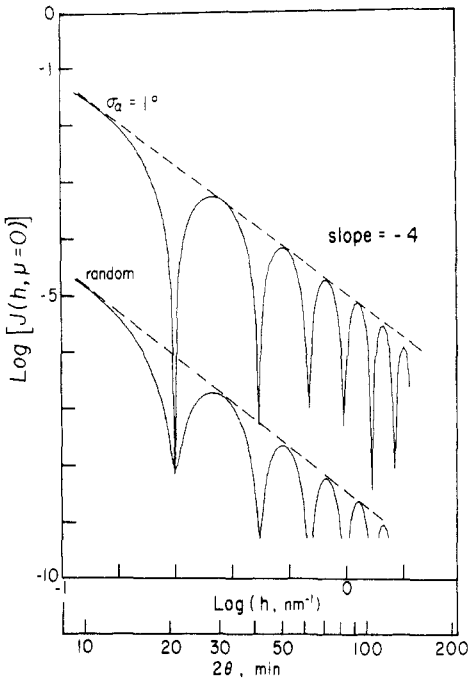

Figure 3. Calculated scattered intensity $J(h,\mu=0)$ for systems with a preferred orientation (σ_α = 1°) and with random orientation: R = 1000 nm, L = 25 nm, σ = 0 nm, σ_L = 0 nm, $\bar{D}$ = 50 nm, and g = 0.5.

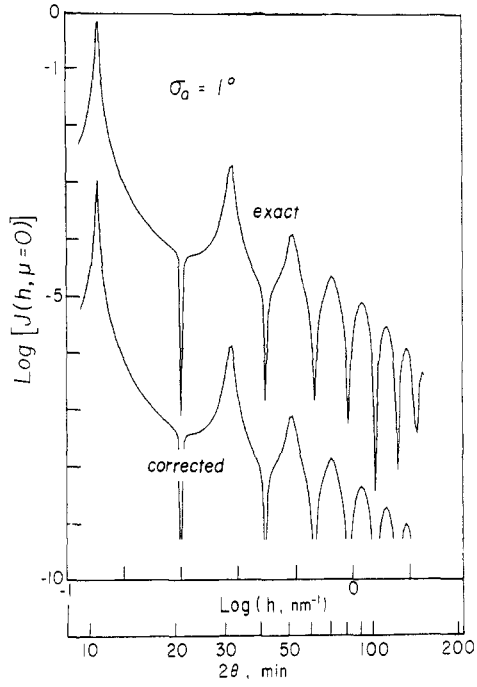

Figure 4. "Exact" (upper) and "corrected" (lower) scattered intensity $J(h,\mu=0)$ for the preferentially oriented system (σ_α = 1°): R = 1000 nm, L = 25 nm, σ_L = 0 nm, σ = 0 nm, $\bar{D}$ = 50 nm, and g = 0.05.

fined by eq I-1 being equal to 0.99, and for $\sigma_\alpha = \infty$ (random orientation), corresponding to $f_\alpha = 0$.

Figure 3 shows the profiles calculated for R = 1000 nm, L = 25 nm, $\bar{D}$ = 50 nm, and σ = 0 nm. These values are typical values for the lamellar microdomain systems. The g factor was set at 0.5 so as to reduce the modulation of the scattering profile due to the lattice factor Z. For this g factor the calculated profiles depend primarily on the particle factor since Z is nearly equal to 1 for h values of current interest. It is clearly seen that the intensity asymptotically decreases according to h^{-4}, *regardless of the degree of orientation.* Thus the result numerically proves eq II-37 and II-41.

Figure 4 shows the calculated scattering curves for the highly oriented grains with σ_α = 1°. The same set of parameters as in Figure 3 was used except for the g factors. The g factor in Figure 4 is 0.05 instead of 0.5 so that the profiles are modulated due to the lattice factor Z. The upper curve is the "exact profile" calculated from eq II-43, while the lower curve is calculated from eq II-28, i.e., by multiplying the h^{-2} factor (Lorentz factor) to the meridional scattering from the perfectly oriented grain (the profile thus calculated being defined as "corrected profile", since it corresponds to the "profile from the perfectly oriented grain" corrected for the Lorentz factor). The two profiles are identical despite the almost perfect orientation, naturally supporting eq II-28. It should be noted that since the volume fraction of one type of the domain ϕ is equal to 0.5, only the odd-order interparticle scattering maxima up to the third-order appear distinctly in the profiles. The maxima with order greater than the third are those corresponding to intraparticle scattering maxima attributed to f_j in eq II-13.

Figure 5 shows the calculated scattering curves for randomly oriented systems with exactly the same set of parameters as in Figure 4. Again it is obvious that the "corrected profile" (upper) is identical with the "exact profile" (the lower curve), which is well expected for randomly oriented systems. All the profiles shown in Figures 4 and 5 asymptotically decrease with h according to h^{-4},

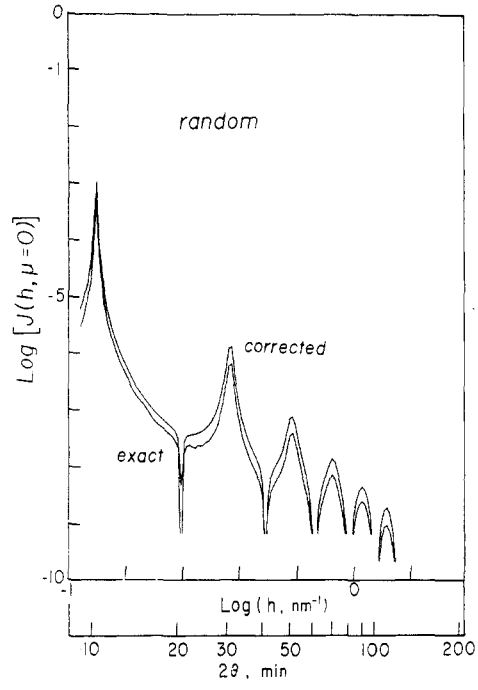

Figure 5. "Corrected" (upper) and "exact" (lower) scattered intensity $J(h,\mu=0)$ for the randomly oriented system having the same set of parameters as in Figure 4.

and hence eq II-37 was proven, irrespective of the degree of orientation.

III. Experimental Section

We shall first describe the method (section III-1) and experimental SAXS profiles (section III-2). The SAXS profiles were then quantitatively compared with the calculated profiles based on the scattering from the perfectly oriented grain corrected for the Lorentz factor (i.e., "the corrected profiles" (section III-3)). For this purpose eq II-31 was used, since the equation was numerically proven to be appropriate to the present systems. The best-fitting

Table I
Sample Characteristics

code	$\bar{M}_n \times 10^{-4}$	wt % PS
L-2	3.1	40
L-7	10.5	46

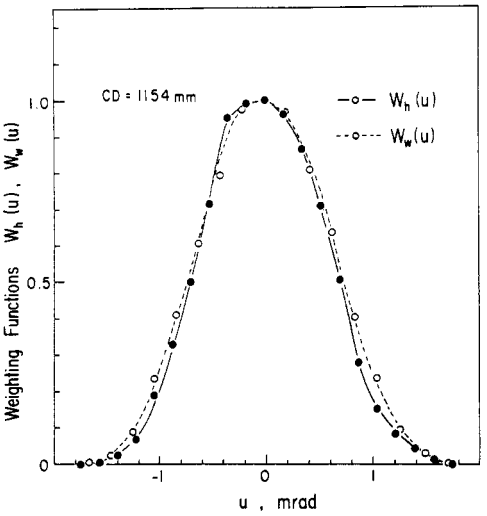

Figure 6. Measured slit-height, W_h, and slit-width weighting functions, W_w, for the camera distance, CD, of 1154 mm.

procedure gives rise to the fundamental structure parameters of the systems. Among the parameters, ϕ (the volume fraction of one type of domain) will be separately discussed in section III-4 and g (g factor) and t (characteristic interfacial thickness) in sections III-5 and -6, respectively, in comparison with the values determined by other methods.

1. Methods. (a) Samples. Two kinds of diblock polymers comprising of polystyrene and polyisoprene were prepared by living anionic polymerization with *sec*-butyllithium as an initiator and tetrahydrofuran as a solvent. The characteristics of these polymers, designated L-2 and L-7, are listed in Table I.

The polymers were cast into films ca. 200 μm thick by pouring ca. 8 wt % toluene solution onto a glass plate in a toluene vapor atmosphere at 30 °C. The films obtained were dried under vacuum for several days until they attained constant weight and then were cut into ribbon shapes of dimension 2 × 15 mm^2. About 20 sheets of the ribbon-shaped films were stacked, and the stacks were used as specimens for X-ray studies. The incident X-ray beam propagates parallel to the film surfaces, the thickness of the specimens along the incident beam being 2 mm.

(b) SAXS Measurements. A rotating-anode X-ray generator (Rigaku Denki RU-200a) and a PSPC system[36,37] were used for measurement of SAXS profiles. A power of 50 kV and 200 mA was used, and Cu Kα radiation (λ = 0.154 nm) monochromatized by graphite crystal was used. In this study we used a point collimation, i.e., two 0.5-mm-diameter pinholes being used for the first and the second collimators at a distance of 400 mm and a 1-mm height-limiting slit placed just before the PSPC probe. The distance between the sample and the detector was 1154 mm for the measurements in the low-angle region and 457 mm for measurements in the tail region.

2. Experimental Results and Discussion. Figure 6 shows the measured slit width $W_w(u)$ and slit height $W_h(u)$ weighting functions for the camera distance of 1154 mm. The figure clearly indicates the optical system is related to a point collimating system, W_h and W_w having the same weighting functions which can be well approximated by

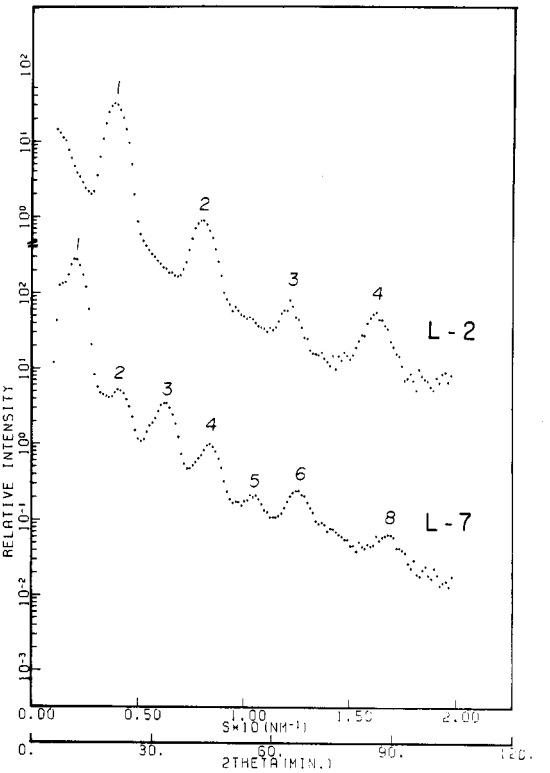

Figure 7. Observed SAXS intensity profiles of L-2 and L-7, respectively, for the small-angle region. The order of each scattering maximum is indicated with the number.

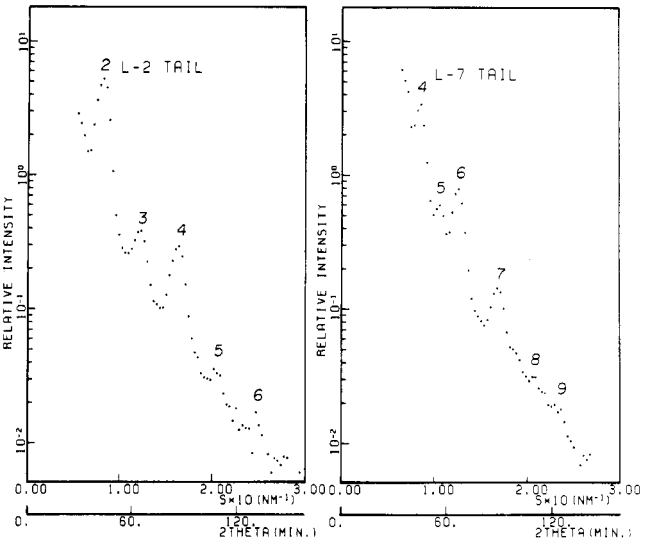

Figure 8. Observed SAXS intensity profiles of L-2 and L-7, respectively, for the tail region. The order of each scattering maximum is indicated with the number.

a Gaussian function with the standard deviations $\sigma_w = \sigma_h$ = 2.024′. Similar but broader profiles were obtained for W_h and W_w for the camera distance of 457 mm with the standard deviations $\sigma_w = \sigma_h$ = 3.16′.

In our previous papers the lamellar microdomains in the solvent-cast films were shown to have *a high degree of orientation* with their normals parallel to the film normal.[5] The second-order orientation factor f_α can be as high as 0.95 for a particular case.[22] In this work, the incident X-ray beam was parallel to the film surfaces of the stacked specimens and the scattered X-ray was detected parallel to the film normal to measure $J(h,\mu=0)$ (the "meridional scattering"). The SAXS profiles in the tail angular region were measured for a long measuring time, typically 12000

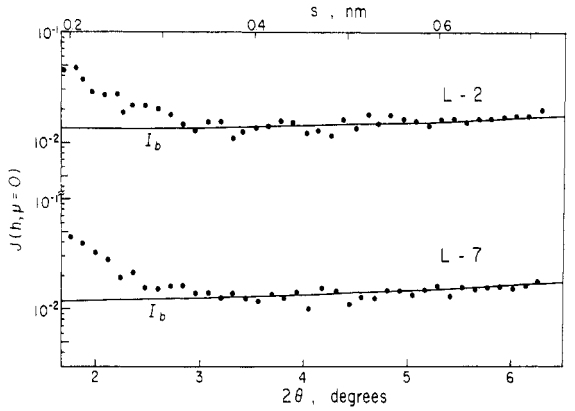

Figure 9. Observed SAXS profiles in the tail region. I_b is the estimated background scattering.

s, in order to reduce statistical errors involved in photon counting and to compensate the reduction of the intensity caused by the point collimation (typical counts for scattered X-ray in this experiments being at least 1000 counts per channel).

Figures 7 and 8 show the "meridional" SAXS profiles of L-2 and L-7 in the small-angle region and the tail region, respectively. All of these profiles were corrected for air scattering and the diffuse background scattering resulting from *the thermal density fluctuations* I_b. The functional form of I_b was assumed to be given by[20]

$$I_b = a + b(2\vartheta)^m$$

and determined as shown in Figure 9.

The measurements with the point collimations enabled us to omit the desmearing procedure of the measured profiles. In Figures 7 and 8, both L-2 and L-7 exhibit multiple-order scattering maxima at the scattering angle $2\vartheta_n$ as given by

$$2\bar{D} \sin \vartheta_n = n\lambda \qquad (n = 1, 2, 3, \ldots) \qquad \text{(III-1)}$$

indicating that the lamellar microdomain structures really exist in both samples. In Figure 8 one can observe clearly the higher order maxima of n = 4, 5, 6, and 7 for L-7 and n = 2, 3, and 4 for L-2.

3. Comparison with Theoretical Results. For simulations of the experimental SAXS profiles with the theoretical ones on the basis of eq II-28, the following attentions were further made. Even in the fine point-collimating system with small σ_w and σ_h, as adopted in this work (Figure 6), the experimental profiles were subjected to the smearing effect.[38] It turns out that the lamellar microdomain systems have usually extremely high uniformity in terms of the identity period D and the size of one type of lamellae L, giving rise to extremely narrow breadths for the scattering maxima with h. Consequently the breadths of the measured scattering maxima are primarily related to the instrumental broadening, i.e., the breadth of the weighting functions, which makes direct applications of the ordinary slit-desmearing procedures impossible due to convergence problems.[38] In order to circumvent this difficulty, the theoretical profiles were smeared with a finite width of the incident beam and compared with the experimental profiles

$$\tilde{J}(h,\mu=0) = \int_{-\infty}^{\infty} W_w(u) J(h-u,\mu=0)\, du \qquad \text{(III-2)}$$

$$W_w(u) = (2\pi\sigma_w^2)^{-1/2} \exp(-u^2/2\sigma_w^2) \qquad \text{(III-3)}$$

Here $\tilde{J}$ *is the smeared theoretical profile.* This procedure neglects smearing due to the lateral overlap (i.e., overlap

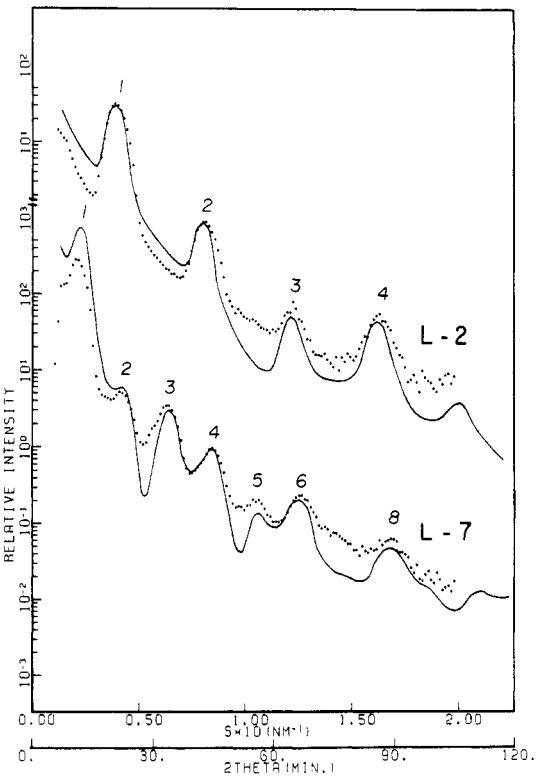

Figure 10. Simulated results for the SAXS profiles in the small-angle region of L-2 and L-7. The dotted lines and the solid lines show the observed and simulated curves, respectively.

in the μ direction) of the scattering patterns from the grains having different orientations, the effect of which may be small because of the small instrumental width $\sigma_w = \sigma_h$, as discussed in section III-2.

In order to conduct simulations of the experimental profiles with the theoretical ones $\tilde{J}$, three more parameters were introduced in addition to R, L, $\bar{D}$, and g as described in sections II-1 and II-5: (i) the standard deviation of the thickness of the domain σ_L from the average $\bar{L}$, (ii) the average number of one type of lamella in the grain $\bar{N}$, and (iii) its standard deviation σ_N.

$$P_L(L) = \exp[-(L - \bar{L})^2/2\sigma_L^2] \qquad \text{(III-4)}$$

$$P_N(N) = \exp[-(N - \bar{N})^2/2\sigma_N^2] \Big/ \sum_{N=1}^{2\bar{N}-1} \exp[-(N - \bar{N})^2/2\sigma_N^2] \qquad \text{(III-5)}$$

The volume fraction of one type of lamellae ϕ is related to $\bar{L}$ and $\bar{D}$

$$\phi = \bar{L}/\bar{D} \qquad \text{(III-6)}$$

Figures 10 and 11 show respectively the best-fitted profiles at the low-angle region and the tail region, where the solid and dotted curves are the theoretical and experimental curves, respectively. The experimental curves at the low-angle region and the tail region were simulated by the same set of the parameters.

The average lamellar identity period $\bar{D}$ was first determined from the angular positions of the first- and higher order maxima. Then the volume fraction or composition ϕ ($=\bar{L}/\bar{D}$) and the composition fluctuation σ_L were determined by matching the experimental and theoretical peak heights. The interfacial thickness t was subsequently determined in such a way that the experimental profiles, especially those at large h, are best fitted with the theoretical ones. All the parameters except $\bar{D}$ were determined by trial-and-error. The parameters thus determined from

Table II
Structural Parameters Determined by the Simulation Method and Comparisons with the Values Estimated by Other Methods[a]

code	$\bar{D}$, nm	g	ϕ_{PS}	$\sigma_{L,PS}$, nm	t, nm	$\bar{N}$
L-2	24.8 ± 0.5	0.030 ± 0.005	0.38 ± 0.01	<0.5	1.9 ± 0.3	
		(0.053)[b]	(0.37)[c]		(1.9)[d]	(12.5)[b]
L-7	47.6 ± 0.5	0.030 ± 0.005	0.43 ± 0.01	<0.5	1.8 ± 0.3	
		(0.052)[b]	(0.43)[c]		(1.8)[d]	(9.7)[b]

[a] The values outside the parentheses were estimated by the simulation method, while those inside the parentheses were estimated by other methods, as follows. [b] Determined from Hosemann's plot as discussed in the text. [c] Determined from elemental analysis. [d] Determined from the systematic deviation of the SAXS profiles at the large-angle tail from Porod's rule.

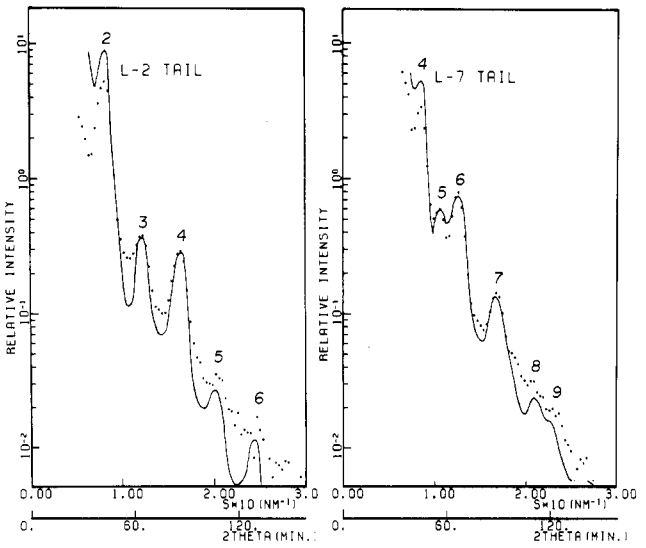

Figure 11. Simulated results for the SAXS profiles in the tail region of L-2 and L-7. The dotted lines and the solid lines show the observed and simulated curves, respectively.

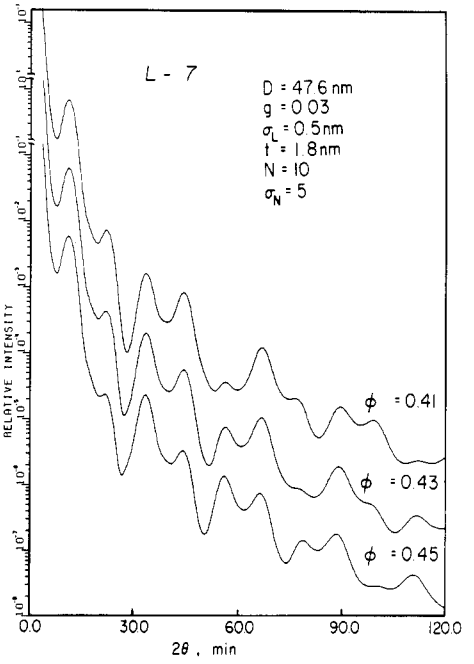

Figure 12. Variation of SAXS intensity profiles with the volume fraction of one type of microdomain ϕ. A slight change of ϕ causes a big change in the relative peak heights of successive maxima.

the simulation method are summarized in Table II and compared with the values estimated by other methods. Accurate determinations of $\bar{N}$ and σ_N by the simulation method are not possible because these parameters affect only the zero-order scattering at scattering angles much smaller than the first-order scattering maximum. In order to make this point clear, we show the average value of the number of the identity period in the grain $\bar{N}$ determined from the Hosemann plot in Table II. $\bar{N}$ is about 10, which is equal to $\bar{N}\bar{D}$ = 250 nm for L-2 and 480 nm for L-7. In the simulation the values $\bar{N}$ and σ_N were arbitrarily chosen as $\bar{N}$ = 10 and σ_N = 5.

The g factors determine the breadth of each scattering maximum. The best-fitting procedure yielded g factors of 0.030 ± 0.005 for L-2 and L-7, suggesting an extremely high uniformity in the domain identity period as given by $\bar{D}_w/\bar{D}_n = 1 + g^2 = 1.0009$, $\bar{D}_w$ and $\bar{D}_n$ being weight-average and number-average D, respectively.[39,44] The g factors were independently determined from the Hosemann plot, as will be discussed in section III-5.

The characteristic interfacial thickness t was estimated to be 1.9 nm and 1.8 nm for L-2 and L-7, respectively. These values agree well with those previously reported. The thickness t was independently measured by using a systematic deviation of the profile in the large-angle tail from Porod's rule, and the value thus estimated was compared with the value estimated by this simulation method in section III-6.

4. Estimation of Volume Fraction ϕ of One Type of Lamellae. As noted in our previous work,[16] the volume fraction of one type of microdomain ϕ (e.g., polystyrene) very sensitively affects the relative peak heights of the profile, allowing accurate estimation of ϕ. Figure 12 shows a typical example of the sensitivity of the profile with ϕ. The parameters other than ϕ were set equal to those for L-7. The parameter ϕ was shifted by ±0.02 from the best-fitted parameters of ϕ = 0.43. Owing to the existence of many higher order scattering maxima, only a little variation of ϕ can be sensitively detected in the variation of the profiles, especially in the variations in relative peak heights. The values of ϕ_{PS}'s thus estimated were in good agreement with those estimated from elemental analyses.[43]

σ_L is also important to determine ϕ. When σ_L is large, the domain thicknesses of one type of the lamellae have large fluctuations, resulting in loss of the characteristic peak height ratios in the SAXS profiles. The upper limit of the σ_L is given in Table II. Physically the fluctuations of polystyrene ($\sigma_{L,PS}$) and polyisoprene domain thicknesses ($\sigma_{L,PI}$) are not independent of each other but are mutually interrelated. It is to be expected that the domain systems should have the following relationships:

$$\sigma_{L,PS} \simeq \sigma_{L,PI} \cong \Delta D \qquad \text{(III-7a)}$$

or

$$\sigma_{L,PS}/\bar{L}_{PS} \cong \sigma_{L,PI}/\bar{L}_{PI} \cong g \qquad \text{(III-7b)}$$

where $\bar{L}_{PS}$ and $\bar{L}_{PI}$ are the average lamellar thicknesses of polystyrene and polyisoprene microdomains. The results listed in Table II seem to satisfy eq III-7b.

5. Estimation of the g factor. The g factor determines qualitatively the number of distinguishable higher order maxima and quantitatively the integral breadth $\delta\beta(n)$ of the nth order maximum. Paracrystal theory[34] gives

$$gn \gtrsim 0.35 \qquad \text{(III-8)}$$

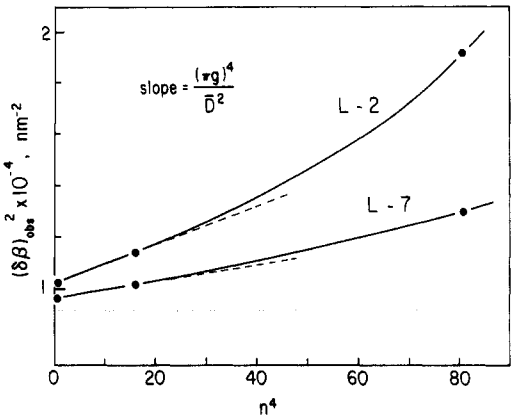

Figure 13. Hosemann's plot of L-2 and L-7. The horizontal dotted line corresponds to the $[\delta\beta_i]^2$ in eq III-10a.

as the criterion for the nth order maximum being indistinguishable from the background scattering, and

$$\delta\beta(n) \equiv \frac{1}{\Delta h}\int_{(n-1/2)\Delta h}^{(n+1/2)\Delta h} J(h,\mu=0)\, dh \qquad \text{(III-9a)}$$

$$\delta\beta(n) = [1 - \exp(-2\pi^2 g^2 n^2)]/2\bar{D} \simeq n^2\pi^2 g^2/\bar{D} \qquad \text{(III-9b)}$$

For L-7 the simulation gave $\bar{D}$ = 47.6 nm and g = 0.03, and hence $\delta\beta(1)$ is expected to be

$$\delta\beta(1) = 1.866 \times 10^{-4}\ \text{nm}^{-1}$$

while the integral width of the incident beam $\delta\beta_i$ is

$$\delta\beta_i = 1.060 \times 10^{-2}\ \text{nm}^{-1}$$

The instrumental broadening $\delta\beta_i$ itself was carefully set to the small value, but yet the domain systems are so regular that $\delta\beta(1)$ is much smaller than $\delta\beta_i$.

$$\delta\beta(1) \ll \delta\beta_i$$

Thus, the peak widths of the observed profiles are due almost entirely to instrumental broadening in our cases.

The g factor is independently determined by the Hosemann plot[34] if both $W_w(h)$ and peak profiles are given by Gaussian functions

$$[\delta\beta(n)]^2 = [\delta\beta(n)]_{obsd}^2 - [\delta\beta_i]^2 \qquad \text{(III-10a)}$$

$$[\delta\beta(n)]^2 = (1/(N\bar{D})^2) + ((\pi g)^4 n^4/\bar{D}^2) \qquad \text{(III-10b)}$$

where $[\delta\beta(n)]_{obsd}$ is the observed integral breadth of the nth order maximum. Figure 13 shows the Hosemann plot for L-2 and L-7. From the slopes the g factors were estimated to be 0.053 and 0.052 for L-2 and L-7, respectively, and from the intercept at n = 0, the sizes of the grain perpendicular to the interface $N\bar{D}$ were estimated to be 3.1×10^2 nm for L-2 and 4.6×10^2 nm for L-7, respectively. Although the $\delta\beta(n)$'s for $n \geq 4$ were measured, they were not included in the plot, because they undoubtedly violate the criterion of $2\pi^2 g^2 n^2 \ll 1$.

Although the g factors estimated here are slightly greater than those determined by the simulation technique (see Table II), the origin of this discrepancy will not be further discussed here.

6. Estimation of the Characteristic Interfacial Thickness t. From the arguments given in section II-4 and subsequent numerical verifications in section II-5, it is obvious that the parameter t affects the asymptotic behavior of the profile at large h (see eq II-35). In the previous papers,[5,16,22] "perfect orientation" of the grain parallel to the film normal was assumed so that the parameter σ, related to the thickness t, was estimated on the basis of

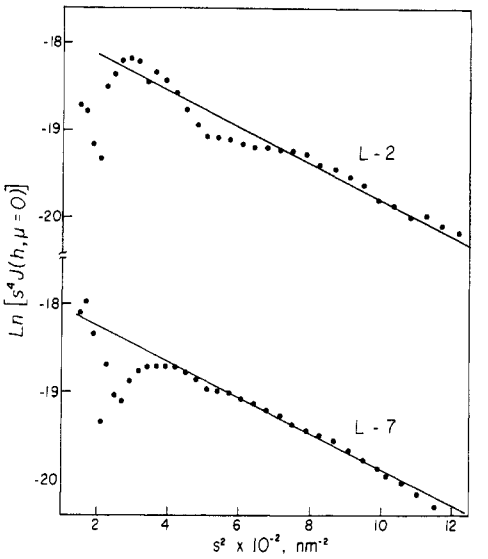

Figure 14. Plot of ln $[s^4 J(h,\mu=0)]$ vs. s^2 to estimate the characteristic interfacial thickness.

$$I_1(h,\mu=0) \sim h^{-2}\exp(-\sigma^2 h^2) \qquad \text{(III-11a)}$$

or

$$\ln [I_1(h,\mu=0)h^2] = \text{const} - \sigma^2 h^2 \qquad \text{(III-11b)}$$

However it was concluded in this study that t or σ for the systems having orientation distribution of the grains, no matter how small the orientational perturbation is from perfectness, should be determined by using the same equation as that for the systems having random orientation distribution

$$J(h,\mu=0) \sim h^{-4}\exp(-\sigma^2 h^2) \qquad \text{(III-12a)}$$

or

$$\ln [J(h,\mu=0)h^4] = \text{const} - \sigma^2 h^2 \qquad \text{(III-12b)}$$

Therefore the values of σ or t were evaluated by using eq III-12b in this work. Figure 14 shows the plots to evaluate the values σ's, from which the values of t were determined by using eq II-6. It should be noted that in Figure 14 s is related to the scattering vector h by eq II-8. The characteristic thickness t thus evaluated was 1.9 nm for L-2 and 1.8 nm for L-7 which was equal, within experimental error to the corresponding value estimated from the simulation method (see Table II).

IV. Concluding Remarks

The scattering equation $J(h,\mu)$ from an uniaxially oriented one-dimensional assembly of lamellar microdomains is derived and compared with $I_1(h,\mu=0)$ from a perfectly oriented one-dimensional assembly. The intensity $I_1(h,\mu=0)$ is the meridional scattering parallel to the assembly axis. It is shown that

$$J(h,\mu) \sim h^{-2} I_1(h,\mu=0) \qquad \text{(IV-1)}$$

irrespective of the sharpness of the orientation distribution if the radius of the domain R is much larger than the thickness of the domain L. This condition is usually satisfied for the block polymers having lamellar microdomains. Equation IV-1, which is well-known for randomly oriented assemblies should be used no matter how small is the orientational perturbation from the perfect orien-

tation. The equation gives Porod's rule at large h, satisfying $hR \gg 1$

$$J(h,\mu) \sim h^{-4} \quad \text{(IV-2)}$$

regardless of the state of orientation distribution, except for the perfect orientation as a singular point.

Equations IV-1 and IV-2 were numerically proven. Equation IV-1 was also proven experimentally, that is, the experimental profiles measured with a *point collimation* can be fitted with the theoretical curves *only when the factor* h^{-2} *(Lorentz factor) is multiplied* with the one-dimensional scattering $I_1(h,\mu=0)$. The simulations of the experimental curves with the theoretical ones yielded important structural parameters, as summarized in Table II. The same values of t (characteristic interfacial thickness) were obtained, within experimental error by the simulations in the small-angle region and in the large-angle tail, as well as by the method involving the analyses of the systematic deviation of the scattering profiles in the large-angle tail from Porod's rule.

Acknowledgment. We are grateful to Prof. H. Kawai for his encouragements on this work. This work is partially supported by a scientific grant from the Asahi Glass Foundation for Industrial Technology.

Registry No. (Styrene)-(isoprene) (copolymer), 25038-32-8.

References and Notes

(1) See, for example: (a) Hoffmann, M.; Kämpf, G.; Krömer, H. Pampus, G. *Adv. Chem. Ser.* **1971**, *No. 99*, 351. (b) Sadron, C.; Gallot, B. *Makromol. Chem.* **1973**, *164*, 301. (c) Folkes, M.; Keller, A. In "Physics of Glassy Polymers"; Haward, R. N., Ed.; Applied Science: Essex, UK, 1973. (d) Gallot, B. *Adv. Polym. Sci.* **1978**, *29*, 87. (e) Hashimoto, T.; Shibayama, M.; Fujimura, M.; Kawai, H. *Mem. Fac. Eng., Kyoto Univ.* **1981**, *43*, 184.
(2) (a) Meier, D. J. *J. Polym. Sci., Part C* **1969**, *26*, 81. (b) Meier, D. J. *Prep. Polym. Colloq., Soc. Polym. Sci., Jpn.* **1977**.
(3) Helfand, E. *Macromolecules* **1975**, *8*, 552.
(4) Helfand, E.; Wasserman, Z. R. *Macromolecules* **1976**, *9*, 879.
(5) Hashimoto, T.; Shibayama, M.; Kawai, H. *Macromolecules* **1980**, *13*, 1237.
(6) Hadziioannou, G.; Skoulios, A. *Macromolecules* **1982**, *15*, 258.
(7) Richards, R. W.; Thomason, J. L. *Macromolecules* **1983**, *16*, 982.
(8) Helfand, E.; Wasserman, Z. R. *Macromolecules* **1980**, *13*, 994.
(9) Mori, K.; Hasegawa, H.; Hashimoto, T.; Kawai, H. to be submitted to *Macromolecules*.
(10) Helfand, E.; Wasserman, Z. R. *Macromolecules* **1978**, *11*, 960.
(11) Hashimoto, T.; Fujimura, M.; Kawai, H. *Macromolecules* **1980**, *13*, 1660.
(12) Bates, F. S.; Berney, C. V.; Cohen, R. E. *Macromolecules* **1983**, *16*, 1101.
(13) Shibayama, M.; Hashimoto, T.; Hasegawa, H.; Kawai, H. *Macromolecules* **1983**, *16*, 1427.
(14) Hashimoto, T.; Shibayama, M.; Kawai, H. *Macromolecules* **1983**, *16*, 1093.
(15) Shibayama, M.; Hashimoto, T.; Kawai, H. *Macromolecules* **1983**, *16*, 1437.
(16) Hashimoto, T.; Nagatoshi, K.; Todo, A.; Hasegawa, H.; Kawai, H. *Macromolecules* **1974**, *7*, 364.
(17) Ruland, W. *J. Appl. Crystallogr.* **1971**, *4*, 70.
(18) Kim, H. *Macromolecules* **1972**, *5*, 594.
(19) Skoulios, A. E. In "Block and Graft Copolymers"; Burke, J. J., Weiss, V., Eds.; Syracuse University Press: Syracuse, NY, 1973.
(20) Vonk, C. G. *J. Appl. Crystallogr.* **1973**, *6*, 81.
(21) Bonart, R.; Müller, E. H. *J. Macromol. Sci., Phys.* **1974**, *10*, 177.
(22) Hashimoto, T.; Todo, A.; Itoi, H.; Kawai, H. *Macromolecules* **1977**, *10*, 377.
(23) Todo, A.; Uno, H.; Miyoshi, K.; Hashimoto, T.; Kawai, H. *Polym. Eng. Sci.* **1977**, *17*, 587.
(24) Todo, A.; Hashimoto, T.; Kawai, H. *J. Appl. Crystallogr.* **1978**, *11*, 558.
(25) Koberstein, J. T.; Morra, B.; Stein, R. S. *J. Appl. Crystallogr.* **1980**, *13*, 34.
(26) Roe, R.-J.; Fishkis, M.; Chang, C. J. *Macromolecules* **1981**, *14*, 1091.
(27) Fujimura, M.; Hashimoto, H.; Kurahashi, K., Hashimoto, T.; Kawai, H. *Macromolecules* **1981**, *14*, 1196.
(28) Hashimoto, H.; Fujimura, M.; Hashimoto, T.; Kawai, H. *Macromolecules* **1981**, *14*, 844.
(29) Roe, R.-J. *J. Appl. Crystallogr.* **1982**, *15*, 182.
(30) Siemann, U.; Ruland, W. *Colloid Polym. Sci.* **1982**, *260*, 999.
(31) Hashimoto, T.; Tsukahara, Y.; Tachi, K.; Kawai, H. *Macromolecules* **1983**, *16*, 648.
(32) Annighofer, F.; Gronski, W. private communication.
(33) Shibayama, M.; Hashimoto, T. unpublished results.
(34) Hosemann, R.; Bagchi, S. N. "Direct Analysis of Diffraction by Matter"; North-Holland: Amsterdam, 1962.
(35) Ruland, W. *Colloid Polym. Sci.* **1978**, *256*, 932.
(36) Hashimoto, T.; Suehiro, S.; Shibayama, M.; Saijo, K.; Kawai, H. *Polym. J. (Tokyo)* **1981**, *13*, 501.
(37) Fujimura, M.; Hashimoto, T.; Kawai, H. *Mem. Fac. Eng., Kyoto Univ.* **1981**, *43*, 224.
(38) See, for example: Guinier, A.; Fournet, G. "Small-Angle Scattering of X-rays"; Wiley: New York, 1955.
(39) Hashimoto, T.; Tanaka, H.; Hasegawa, H. *Macromolecules* **1985**, *18*, 1864.
(40) Hashimoto, T.; Kawai, H. *Polym. Prepr. (Am. Chem. Soc., Div. Polym. Chem.)* **1979**, *20*, 28.
(41) Here the grain is equivalent to the lamellar stack, but the term "grain" emphasizes that they are structural units that fill the whole sample space with impingements, the boundaries of the impingements being called "grain boundaries". Orientation of the lamellar domains are coherent within the grain but incoherent between different grains.
(42) In eq 21a individual grains are assumed to give "independent scattering". Since the size of the grain is a few microns and a few tens of microns in the direction parallel and perpendicular to the z axis (see Figure 1), respectively, the interference of the scattered X-rays between different grains is significant only at extremely small scattering angles inaccessible to normal scattering experiments. Thus the intergrain interference effect is negligible at the scattering angles of interest, and hence the total scattered intensity is given by a sum of the intensities from the individual grains.
(43) It should be noted that the SAXS method gives only the volume fraction of either one of the two kinds of domains (PS or PI domains). It is needless to say that one needs independent information in order to identify the domain corresponding to the volume fraction.
(44) The g values for the lamellar systems, g_{lamella}, were estimated to be 0.03. The small but nonzero g values indicate extremely high uniformity of D in the lamellar microdomain system, as described in the text. A rigorous determination of g values for spherical domain systems g_{sp} has not yet been reported. The g_{sp}'s are also small, as qualitatively described in ref 39, but seem to be greater than the g_{lamella}, which may reflect strong nonequilibrium effects encountered in the formation of the spherical domains.[13]